On Board Dual Active Bridge Converter for Electric scooter

By

Muhammad Saim ul Haq Kundi
Enrollment No. 01-133222-055

Hamna Ahmed
Enrollment No. 01-133222-023

Supervised By

Dr. Asad Waqar

Session 2022–26

A Report submitted to the Department of Electrical Engineering,
Bahria University, Islamabad.
In partial fulfillment of requirement for the degree of BS(EE).

Certificate

We accept the work contained in this report as a confirmation to the required standard for the partial fulfillment of the degree of BS(EE).

_____.

Head of Department

_____

Supervisor

_____.

Internal Examiner

_____

External Examiner

Dedication

I am extremely grateful to attribute this success to my parents, whose unbending support has been the backbone of my experience.Endless patience, silent sacrifices and profound faith in my capabilities have helped me to overcome all the obstacles I had to overcome.They have always stood by my side, and even when I have been in doubt they have given me strength, and when I have been in need, they have given me hope, without my needing their help to be recognized.The most inspiring thing to me has been their pure prayers and unconditional love.Not only is this a milestone of mine but of all they have done to me.I am eternally grateful to their presence, directions, and the beliefs that they have sparked in my life.

Acknowledgments

I would wish to acknowledge all those who assisted in making this thesis a success. I would like to express my gratitude to my supervisor, Dr. Asad Waqar, whose positive feedback, support and guidance were invaluable in this study. His experience and mentorship of him had a very great influence on the quality and direction of this work.

I also would like to thank my great faculty, the great faculty of Bahria University, which provided me with the knowledge, skills, and academic base that I needed to achieve this study. They have a commitment to excellence in teaching and this has really helped me in matters intellectual as well as in professional matters.

I would like to seriously thank my parents and my family as they always encouraged, supported and prayed to me and it has become my great source of strength and inspiration to go on with my academic journey. I also like how my project partner cooperated, was dedicated and worked as a team which also helped to contribute to the success of this project.

And, finally, I wish to acknowledge the support, the advice, and the help of my friends, and everyone, who, in one way or another, supported, advised, and helped me at various stages of this work that I have accomplished.

Abstract

After the recent increase in the popularity of electric scooters, which are small, earth friendly and more effi- is on the increase. cient onboard chargers. Despite being big in size, powerful chargers are big in size. do not have the efficiency to power small cars such as scooters, onboard. chargers should be tiny, powerful, low cost, and dependable. This thesis proposes a design and model of a small onboard charger. on a Dual Active Bridge (DAB) converter. The proposed system uses a high-frequency (HF) isolated DC-DC converter, fitting power and galvanic isolation simultaneously and enabling power transfer between them easily. between the battery storage system and the source. For unidirectional oper- This modulation scheme is called Single Phase Shift (SPS) modulation scheme and used so as to simplify. the control strategy, reduce switching losses and reduce computational. overhead, which renders it suitable to deploy with a low-priced embedded. controller. The impact of non-ideal terms, such as leak- is also considered in the study. inductive coupling with age, switching losses and power-delivery parasitance. and voltage regulation. It is the MAT- system that is modelled and simulated. LAB/Simulink to check its performance in a variety of load and input. voltage conditions. In addition, a realistic prototype is created, featto make a full-bridge circuit of MOSFETs a high-frequency trans- former, and an Arduino-based controller to produce PWM (Pulse Width). Modulation) signals. The special emphasis is made on optimization of the trans- old design and switching approach to reduce the output voltage ripple. It is proposed to work, both in simulation and experimental results. system steadily DC output, efficiency in power transfer and minimized. size, it can be used extensively in the applications of electric scooters. The design created can provide a viable approach to overcome the constraints of current charging systems.

Contents

List of Figures

List of Tables

Chapter 1

Introduction

1.1 Background

The transport sector is rapidly heading towards electric vehicles as we need to lessen pollution and consume less fuel such as petrol and diesel. Electric cars are increasingly becoming widespread with the improvement of technology and their increasing ease of operation. The shift is also being supported in many countries, to achieve a cleaner and greener transportation.One of the most commercially feasible solutions has been identified as electric vehicles (EVs), which are delivered throughout the world with an increasing rate of 32.4 percent annually as of 2025. [1]. Such an unprecedented increase has resulted in an urgent need to have very efficient, reliable, and two-way EV charging infrastructure. [5].

The heart of EV charging systems is the power electronics interface between the grid and vehicle battery. Standard unidirectional chargers do not have the ability to support current smart-grid applications that enable the ability to return stored energy in the vehicle. [6]. Bidirectional DC–DC converters that are isolated are thus critical building blocks of the next generation EV charging stations.

Among the many forms of bidirectional isolated DCDC converter topology discussed in the literature, the Dual Active Bridge (DAB) converter has become the most popular topology because of its symmetrical structure, galvanic isolation, intrinsic soft-switching property and high power density. [2, 7].De Doncker, Divan, and Kheraluwala were the first to suggest the DAB. [7]. Since that time it has found widespread application in automotive and renewable energy and energy storage. [6].

Figure 1.1 illustrates the global growth trend in EV adoption, underscoring the urgency for advanced power electronic solutions.

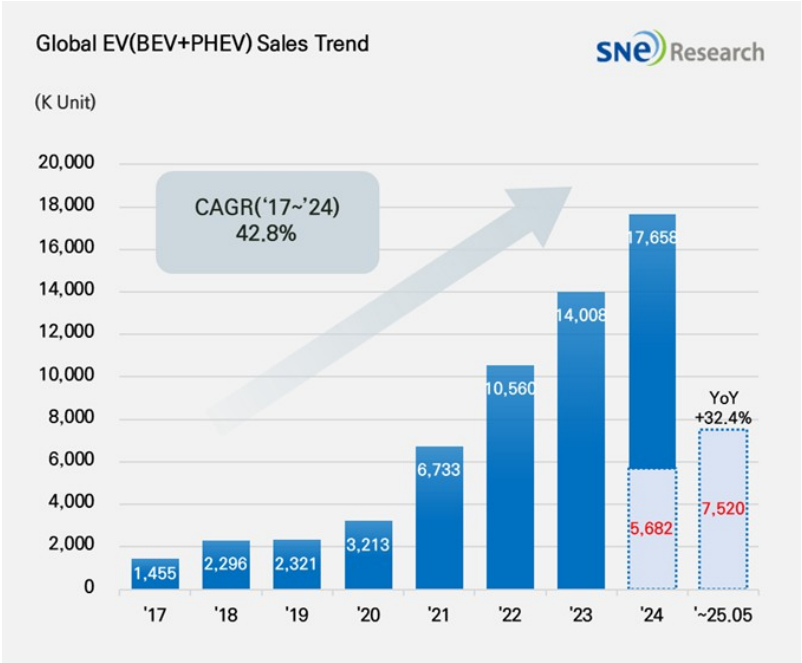

Figure 1.1: Growth of electric vehicle [1].

Figure 1.2 shows the basic DAB converter circuit topology con- comprising two complete H-bridges connected with a high frequency isolation. transformer and series inductance.

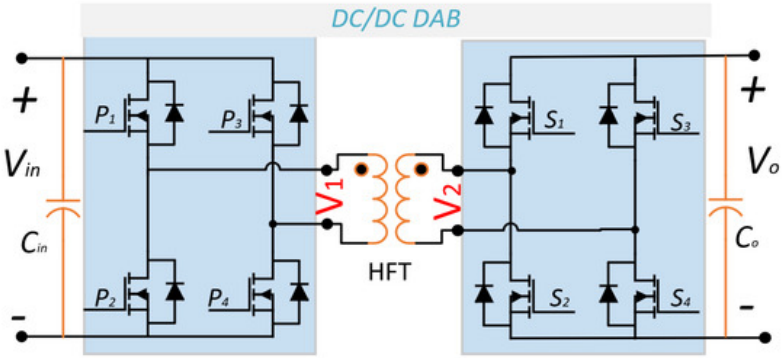

Figure 1.2: topologies [2].

Figure 1.3 illustrates the single-phase DAB operating modes under different phase-shift conditions, showing the inductor current waveforms for

forward and reverse power flow.

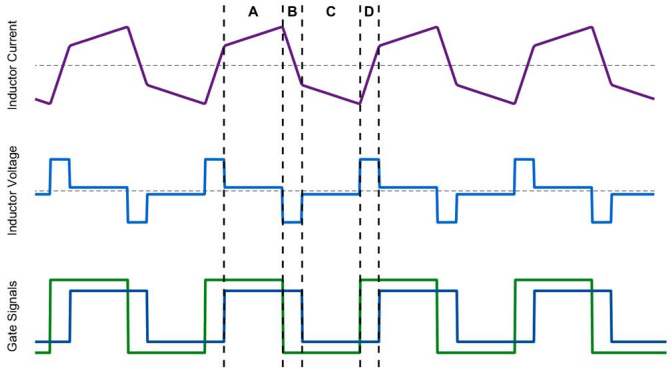

Figure 1.3: Single-phase operation [3].

1.2 Problem Description

Contemporary EV charging stations predominantly rely on unidirectional power conversion, which prevents energy recovery from vehicle batteries back to the grid [5]. Furthermore, conventional hard-switched DC–DC converters suffer from significant switching losses at higher frequencies, limiting achievable power density and converter efficiency [4].Soft-switching methods, like Zero Voltage Switching (ZVS), can reduce these losses, but to implement ZVS over a wide operating range in DAB converters, it is necessary to carefully design the dead time, series inductance and modulation strategy. [8, 9].

The dead-band effect in DAB converters is a well-documented challenge: incorrect dead-time selection leads to either shoot-through conditions or loss of ZVS, both of which degrade converter performance [8]. Existing solutions range from analytical ZVS boundary calculations to advanced modulation strategies that dynamically adjust phase shift to maintain soft-switching [10, 11]. Despite the availability of high-frequency simulation tools such as MATLAB/Simulink , hardware-validated results at the undergraduate level remain sparse, motivating the present work.

1.3 Objectives

The aims of this project are:

- To create a small and efficient Dual Active Bridge (DAB) converter. to be used in charging onboard electric scooter.
- In order to model and test the performance of the proposed system in MATLAB/Simulink.
- To obtain a constant DC output that can be used to charge batteries (around 80 V).
- To be safely and reliably operated, galvanic isolation and controlled power transfer.
- To demonstrate that the low-cost and lightweight electric scooter onboard charging solution is valid.

1.4 Project Scope

The design, simulation, and hardware implementation of a single-phase Dual Active Bridge (DAB) DC-DC converter with Single Phase Shift (SPS) control is explained in this project. The method for transferring power devised by Krismer and Kolar has been employed in the design keeping in mind the operating voltage range and switching frequency. [4].ZVS analysis framework follows Shi et al. [8] and the closed-form ZVS modulation solution of Everts [9]. The design of the transformer is based on the experience of the toroidal transformer design and incorporates ferrite cores to operate the transformer with high frequency operation. [11] are considered as good directions of future work and are not applied in the hardware prototype at hand.

Chapter 2

Literature Review

The DAB converters spans over three decades and encompasses foundational circuit analysis, modulation strategies, hardware design, control systems, and application-specific implementations. This chapter provides a structured review of the most relevant works, identifying the research gaps addressed by the present project.

2.1 Foundational Work and Circuit Analysis

De Doncker, Divan, and Kheraluwala initially proposed the DAB converter. [7]as a high-power, two-way isolated, DC-DC converter with phase-shift modulation between two complete H-bridges. This masterpiece defined the operating principle that is used in all other bridges: The higher the phase shift angle between two bridges, the higher the proportion of power transfer. Kheraluwala later characterised the single-phase performance at 50 kW. [12], who demonstrated soft-switching properties, low component stress, and bidirectional power flow.

Krismer completed the most comprehensive analytical treatment of the DAB in his PhD thesis [2], developing accurate loss models, small-signal models, and optimal modulation trajectories. This work remains the standard design reference for DAB converters.

Krismer and Kolar have published the accurate derivation of the power loss model of the same automotive prototype with explicit separation of conduction losses and switching losses, transformer core losses, and gate driver losses. An equivalent correct small-scale model that could be used to design the digital PI controller was obtained in [13]. Zhao et al. [13] offered a persuasive summary of the DAB as the topology of choice when converting power systems with high frequencies to linking topologies, contrasting it with other isolated bidirectional topologies.

2.2 Modulation Strategies

The main handle by which the power flow, efficiency and soft-switching range of the DAB converter are determined is modulation. The easiest, Single Phase Shift (SPS) scheme, employs one control variable and formed the foundation of the original DAB proposal [7].Although SPS is easy to set up, its ZVS range becomes considerably smaller when operating in light-load conditions, or wide-voltage-conversion-ratio conditions [3, 10].

To overcome these limitations, more advanced modulation strategies have been developed. Hou et al. [10] provided a minimum-current-stress scheme with unified phase-shift controlprovided a minimum-current-stress scheme with unified phase-shift control. Huang et al. [14] presented a unified TPS control framework that minimises circulating current stress while maintaining soft-switching, and Garry et al demonstrated that TPS yields a measurable improvement in overall efficiency compared to SPS in automotive-grade DAB converters. Wu et al. [11] further developed a unified optimal control strategy that spans multiple modulation modes seamlessly. Krismer and Kolar [15] obtained a closed-form solution to the minimum conduction loss modulation of DAB converters, which offers directly applicable design information. The current project uses SPS as the baseline and TPS as the future work.

2.3 ZVS Analysis and Dead-Time Design

The important soft-switching process in DAB converters is Zero Voltage Switching (ZVS), which removes the switching losses in the turn-on. To accomplish ZVS, the inductor current must charge and discharge the MOSFET output capacitances Coss at the start of the dead-time period before the arrival of the gate signal. [8,9]. Shi et al. [8] derived accurate analytical ZVS boundaries for DAB converters under SPS modulation, explicitly accounting for the deadband effect — the distortion introduced by finite dead time on the voltage waveforms. Their work shows that ZVS boundaries are

strongly influenced by the dead-time value, the transformer magnetising inductance, and the operating voltage ratio [8].

Liu et al.extended this analysis by incorporating the nonlinear voltage-dependent capacitance of modern power MOSFETs into the ZVS range calculation, providing a more accurate boundary than linear approximations. Everts [9] obtained an analytical in a directly employable closed-form. solution to efficient, full-operating-range ZVS modulation, including the nonlinear parasitic output capacitances of the switches, to be com- full commutation of bridge legs. Krismer and Kolar [15] developed power loss models that explicitly separate conduction losses from switching losses, enabling dead-time optimization for maximum efficiency. In the present project, dead-time values of 5000 ns, 7000 ns, and 9000 ns are experimentally tested to determine the optimal value for the designed prototype.

2.4 Hardware Design and High-Frequency Magnetics

The practical realisation of a DAB converter requires careful design of the high-frequency transformer, gate drive circuitry, and MOSFET selection. Krismer and Kolar [4] presented an efficiency-optimised design methodology for the automotive 1 kW DAB converter, using two planar E58 ferrite cores, of frequency 10 kHz, and an optimised turns ratio of $n = 127{:}34$ with $L = 22.4\,\mu$H under the optimised modulation scheme, demonstrating that average efficiency rises from 89.6% (SPS) to 93.5% (optimised modulation). He and Khaligh performed a comprehensive comparison of 1000W isolated topologies for bidirectional EV charging, providing practical design guidelines for the transformer and passive components.

Inoue and Akagi [6] demonstrated the DAB converter for a 3300V/6600V medium-voltage conversion of power system, validating the topology's suitability for high-voltage battery-interfaced applications. Shakoor et al described the design and testing of a high frequency toroidal transformer in solid-state transformer applications, giving directly applicable information

in the design of the transformer in the current work. The same research group [16] addressed power quality optimisation in DAB converters. Hannannavar and Shivalli provided a design and implementation guide for a DAB converter specifically targeting battery charging, which served as a hardware implementation reference for this project.

2.5 Control Systems

In addition to modulation, closed-loop control is necessary in the control of the output voltage and current of the DAB converter in response to changing load and input conditions. Krismer and Kolar obtained a small-signal model of the DAB that is correct and supports systematic PI and model-based controller design and executed on a digital signal processor (DSP) on the automotive prototype. Wu et al. [11] proposed unified optimal control that spans multiple modulation modes, providing smooth transitions without mode-switching transients.

2.6 Applications in EV Charging and Energy Storage

Yilmaz and Krein [5] offered an in-depth overview of battery charger topologies and charging infrastructure of plug-in electric and hybrid vehicles, making the DAB the topology of choice in Level 2 and DC fast charging.. Inoue and Akagi [6] proved bidirectional isolated DC–DC conversion as the main circuit in a medium-voltage power conversion system, and directly associated with the V2G charging scenario. Li et al. focused on efficiency optimisation under a broad voltage conversion ratio, which is directly of interest to EV charging when the battery voltage changes greatly with state of charge. Zhao et al. [17] presented a review of the latest, holistic survey of DAB soft-switching methods and circulating current minimisation, which is the state of the art.

2.7 Summary and Research Gap

The DAB converter has been repeatedly cited in the literature as the most suitable topology to use in bidirectional, isolated EV charging. There are well-set tools of ZVS boundary calculation, loss modelling, and modulation optimisation. Nonetheless, lower-level hardware-validated results, especially dead-time sensitivity analysis, are scarcely found in the open literature. The current project is filling this gap by demonstrating and experimentally confirming a DAB prototype, experimenting with three dead-time values (5000 -1, 7000 -1, 9000 -1) and comparing experimental switching waveforms to the simulations. This gives a tangible, repeatable hardware reference that matches the theoretical models defined in. [2, 8].

Chapter 3

Requirement Specifications

3.1 System Exixtance

Present-day EV charging stations principally rely on unidirectional AC-DC converters and then an isolated DC-DC step . These systems are known to have a number of limitations:

- They do not support Vehicle-to-Grid (V2G) energy return, wasting stored energy [6].
- High switching losses are caused by hard-switching operation, which restricts efficiency and power density. [4].
- Efficiency drops significantly at partial load conditions, as documented for SPS-modulated DAB converters where average efficiency is only 89.6% [4].
- Most low-cost designs do not galvanically isolate the grid and the vehicle.

3.2 Proposed System

The suggested system is a galvanically isolated, bidirectional DAB DC-DC converter, which is founded on the topology developed by De Doncker et al. [7] and further developed by Krismer and Kolar [2]. The system supports:

- Bidirectional power flow (G2V and V2G modes) [3, 13].
- ZVS operation over a dead-time range of 5000–9000 ns using SPS modulation [8, 9].
- Hardware implementation with a custom high-frequency toroidal transformer .

3.3 Requirement Specifications

Table 3.1 gives the main design requirements of the DAB converter. The design methodology of Krismer and Kolar is used to derive the values. [2,4], specifically the 1000W automotive prototype documented in those works. The switching frequency of 100 kHz was selected by Krismer and Kolar based on skin-effect and switching-loss trade-off analysis and is adopted here [4].

Table 3.1: Specifications Design

Parameter	**Description**	**Value**
V_{input}	Input DC Voltage (HV port, nominal)	310 V
V_{output}	Output DC Voltage (LV port, nominal)	82 V
P_{rated}	Rated Power	1 kW
f_{sw}	Switching Frequency	10 kHz
L_s	Series Inductance (SPS modulation)	26.7 μH
n	Transformer Turns Ratio (SPS)	127:34
Dead Time	Gate Dead Time Range	5000–9000 ns

3.4 Case

3.4.1 Use Case 1: Grid-to-Vehicle (G2V) Charging

Actor: EV Battery Pack
Description: The DC bus has power flowing through the DAB converter to charge the EV battery as outlined in [5].
Precondition: EV is connected and battery is below target charge level.
Post-condition: Battery is charged to target voltage.

3.4.2 Use Case 2: Vehicle-to-Grid (V2G) Discharge

Actor: Grid / Load
Description: The bidirectional DAB topology allows power to flow out

of the EV battery to the DC bus. [6, 7]. Inverting the phase shift, i.e. changing the sign of the phase shift, is a reversal of the power flow. [3, 13].
Precondition: EV is connected and battery is sufficiently charged.
Post-condition: Power is delivered to the grid or local load.

3.4.3 Requirements for Non-Functional

- **Efficiency:** converter Will achieve a target efficiency of $\geq 90\%$ at rated power, benchmarked against the 89.6% (SPS) to 93.5% (optimised) range reported by Krismer and Kolar [4].
- **Safety:** Galvanic isolation shall be maintained between primary and secondary sides at all times [6].
- **Reliability:** ZVS shall be maintained over the specified dead-time range per the analysis in [8, 9].
- **Scalability:** The design shall be extensible to higher power ratings following the methodology in [2].

Chapter 4

Design

4.1 System Architecture

The DAB converter comprises two full-bridge stages of inverter coupled. via high-frequency isolation transformer and a series inductance. Ls, as laid down in. [2, 7]. The main bridge is used to convert the DC input voltage to a high frequency square wave. This is passed on the transformer and recreated on the secondary bridge. The power flow magnitude and direction is controlled by phase-shift control between the two bridges. [3, 13].

Figure 4.1 Presents the block diagram of the entire DAB converter system.

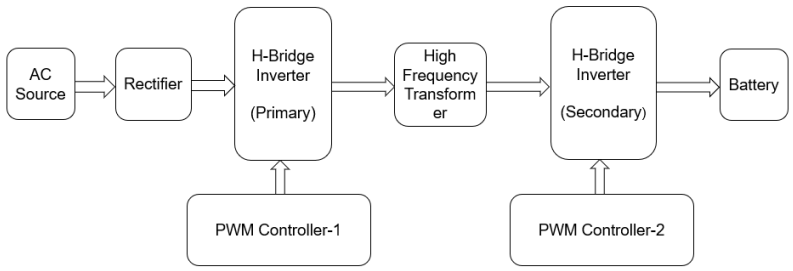

Figure 4.1: Block Diagram of Dual Active Bridge (DAB) Converter.

4.2 Design Constraints

- The 100-kHz switching frequency is limited by the propagation delay of gate drivers and the loss in transformer cores, which are in line with the reasons of frequency selection proposed by Krismer and Kolar. [4], who chose this frequency based on skin-effect and proximity-effect analysis.
- ZVS must be maintained at the nominal operating point to avoid switching losses [8, 9].
- Component values are chosen to ensure ZVS over dead times of 5000–9000 ns.

- The transformer shall be designed with minimum leakage inductance variation, following [**?**].

4.3 Design Methodology

The design follows a three-stage approach based on established literature:

1. **Analytical Design:** The SPS power transfer equation, as derived in Krismer's PhD thesis [2] and also presented in [3]:

$$P = \frac{n \cdot V_1 \cdot V_2}{2\pi f_{sw} L_s} \phi \left(1 - \frac{|\phi|}{\pi}\right) \tag{4.1}$$

   is used to size L_s for the specified power rating. For the design parameters $n = 19$, $V_1 = 310$ V, $V_2 = 80$ V, $f_{sw} = 10$ kHz, and $P_{rated} = 1000W, this yields \mathrm{L}_s = 26.7\,\mu\mathrm{H}$ under SPS modulation [4].

2. **Simulation:** MATLAB/Simulink simulation of the converter is done to check waveforms and ZVS limits prior to constructing hardware.

3. **Hardware Prototyping:** PCB design and component selection are performed, with the transformer design following in [4] and switching device selection following the criteria established in [4].

4.4 Top-Level Design

4.4.1 Logical View

The system is decomposed into the following functional subsystems [2]:

- **Primary H-Bridge:** Four MOSFETs switching at $f_{sw} = 10$ kHz with dead-time control [8].
- **HF Transformer:** Galvanic isolation and scaling of voltages with turns ratio. $n = 127{:}34$ (SPS) [4].
- **Series Inductor $L_s = 26.7\,\mu$H:** Controls power transfer via phase shift ϕ [2, 3].

- **Secondary H-Bridge:** Synchronous rectification for bidirectional operation [11].
- **Gate Drive Circuit:** Generates isolated, dead-time-controlled drive signals [8].
- **Control Logic:** Implements SPS modulation [10].

4.4.2 Process View

Gate signals are generated by a microcontroller with precise dead-time insertion. The control loop reads output voltage and adjusts ϕ accordingly, following the closed-loop framework in [9]. Interrupt-driven ADC sampling ensures low-latency feedback.

4.5 Component-Level Design

4.5.1 MOSFET Selection

MOSFETs are selected based on V_{DS}, $R_{DS(on)}$, and C_{oss} to ensure complete resonant charging/discharging of output capacitances within the specified dead time for ZVS [9]. For the HV side, Krismer and Kolar used the SPW47N60CFD device; for the LV side, IRF2804 devices were used in parallel [4]. The present prototype follows an equivalent selection strategy appropriate for the reduced-scale test setup.

4.5.2 Transformer Design

Table 4.1 summarises key transformer parameters, designed following the methodology in [4]. The core material is ferrite, consistent with Krismer and Kolar's use of two planar E58 ferrite cores operating at 100 kHz [4].

Table 4.1: Transformer Design Parameters [4].

Parameter	**Value**
Core Material	Ferrite (toroidal)
Turns Ratio (n)	127:34 (SPS modulation)
Switching Frequency	100 kHz
Series Inductance L_s	26.7 μH

4.6 Database Design

Not applicable for this hardware-based power electronics project. All simulation and experimental data are stored in structured `.csv` files and oscilloscope exports for post-processing, consistent with the data management approach in .

4.7 Design

The control interface is implemented via a serial terminal for real-time monitoring of phase shift angle, measured voltages, and calculated power, following the approach described in.

4.8 External Interfaces

- **DC Bus (Input):** Regulated DC supply at 340 V representing the grid-side rectifier output [5].
- **EV Battery / Load (Output):** Resistive load bank at 12 V emulating battery impedance during testing .
- **Oscilloscope:** Waveform capture of gate signals and inductor current [8].
- **Microcontroller/DSP:** SPS gate signal generation with configurable dead time .

Figure 4.2 Displays the DAB simulation block diagram in MATLAB/Simulink.

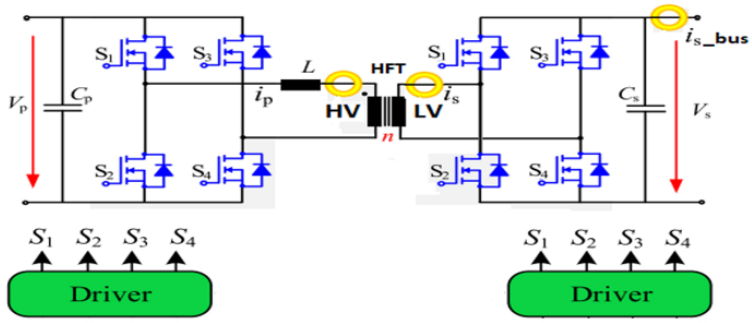

Figure 4.2: MS visio Design

Chapter 5

Implementing System

5.1 System Architecture

The hardware prototype is implemented following the design methodology established by Krismer [2] and the battery charger implementation guidelines of Hannannavar and Shivalli .

- One of the main full H-bridges is made with power MOSFETs that are chosen on the basis of low $Coss$ to allow ZVS.
- A custom-wound high-frequency toroidal transformer, designed following, with turns ratio $n = 19{:}1$ and series inductance $L_s = 26.7\,\mu$H consistent with the SPS design of Krismer and Kolar [4].
- A secondary full H-bridge for synchronous rectification [11].
- Isolated gate drivers with configurable dead time for each bridge [8].
- A microcontroller generating SPS PWM signals at $f_{sw} = 10$ kHz with dead-time values of 5k ns, 7k ns, and 9k ns [8, 9].

Figure 5.1 shows the complete hardware implementating DAB converter.

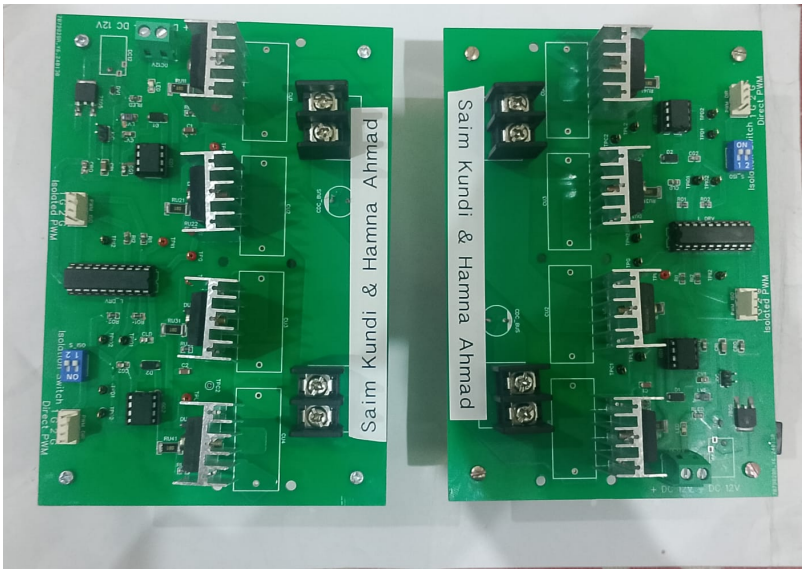

Figure 5.1: Hardware Implementation

Figure 5.2Demonstrates the prototype high-frequency toroidal transformer.

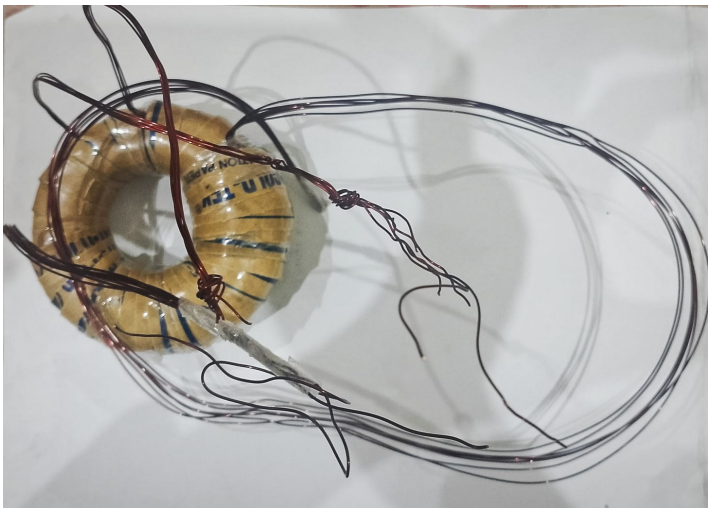

Figure 5.2: HF Transformer.

5.2 Tools and Technology Used

- **Simulation:** MATLAB/Simulink for schematic capture and waveform post-processing.
- **PCB Design:** KiCad (open-source PCB design tool).
- **Microcontroller:** STM32 series ARM Cortex-M microcontroller for PWM generation with configurable dead time.
- **Measurement:** Digital oscilloscope for switching waveform capture [8].

5.3 Development Environment / Languages Used

- **Programming Language:** C/C++ embedded firmware.
- **IDE:** STM32CubeIDE.
- **Document Preparation:** LaTeX (Overleaf).

5.4 Processing Logic / Algorithms

5.4.1 Single Phase Shift (SPS) Modulation

In SPS modulation [7], both switches are at the switch frequency $f_{sw} =$ 10 kHz. The angle of delay between the primary and secondary bridge gate signals is the angle of phase shift phi which defines the strength and direction of power transfer. The equation of power transfer, which is rigorously obtained by Krismer and Kolar in Chapter 3 of the PhD thesis. [2] and also presented in [3], is:

$$P = \frac{n \cdot V_1 \cdot V_2}{2\pi f_{sw} L_s} \phi \left(1 - \frac{|\phi|}{\pi}\right) \tag{5.1}$$

where $n = 19$ is the ratio of transformer turns, $V_1 = 310$ V and $V_2 =$ 80 V are primary and secondary DC voltages, and $L_s = 26.7\,\mu$H is the series inductance [4]. This equation also implies that reversing the sign of ϕ reverses power flow, enabling V2G operation [3, 13].

5.4.2 Dead Time Insertion

To eliminate shoot-through, dead time is added between the turn-off of one MOSFET and the turn-on of its complementary switch. ZVS occurs when the inductor current fills and empties the MOSFET body capacitances during this dead-time phase before the gate signal reaches it. Evertsderived that charge needed to commutate the nonlinear parasitic output capacitances of the switches had to be induced by the inductor current in the dead-time interval. According to the analysis by Shi et al. [8], dead-time values of 5000 ns, 7000 ns, and 9000 ns are evaluated to determine the optimal setting for the designed prototype.

5.5 Application Access Security

Gate drive signals are restricted to the dedicated microcontroller output pins with hardware interlock logic to prevent simultaneous conduction, fol-

lowing safe design practices outlined in [2]. Over-voltage and over-current protection circuits are implemented to safeguard the converter during abnormal conditions.

5.6 Database Security

All experimental data (oscilloscope screenshots and CSV exports) are stored locally and backed up to university cloud storage. No remote access or networked database is used in this project.

Chapter 6

System Testing and Evaluation.

project testing was performed in both simulation (MATLAB/Simulink) and on the hardware prototype, following the evaluation approach recommended by Krismer [2] and validated against the ZVS boundary analysis of Shi et al. [8]. The primary metrics evaluated are ZVS achievement, switching waveform overlap (dead-band compliance), and bidirectional power flow verification.

6.1 Test Setup

primary side connected with rectifier bridge which convert 220VAc to 310V Dc $V_1 = 310$ V.A load bank that was resistive was connected to the secondary side to represent battery impedance. [**?**]. The waveforms in the gates and inductor current were recorded on an oscilloscope in dead times of 5000ns, 7000ns and 9000ns. The range was chosen according to the ZVS boundary analysis of the designed.$L_s = 26.7\,\mu$H and MOSFET C_{oss} values [8, 9].

6.2 Primary Side Switching Waveform Analysis

Figures 6.1–6.6 show the primary side switching signals and overlap analysis at each dead-time value. The results are interpreted with reference to the ZVS criteria established in [8, 9].

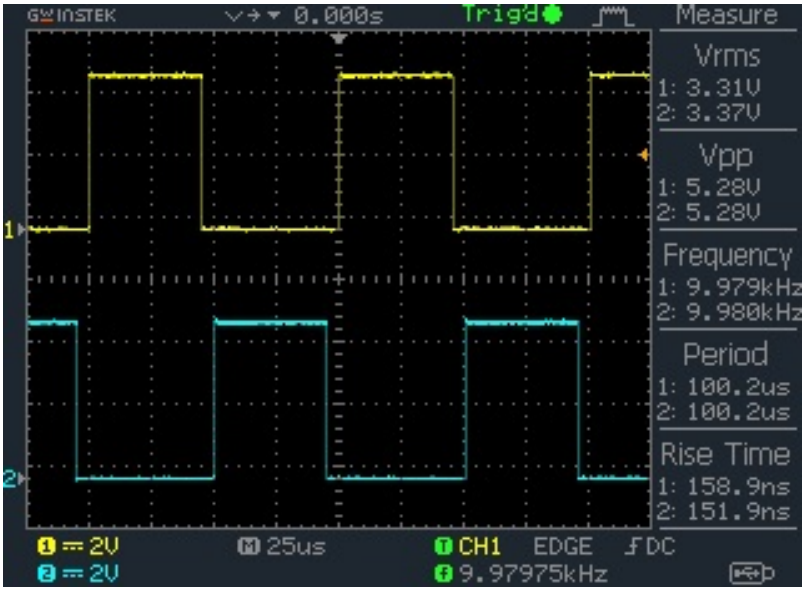

Figure 6.1: Main side switching signals at 5000 ns dead time. .

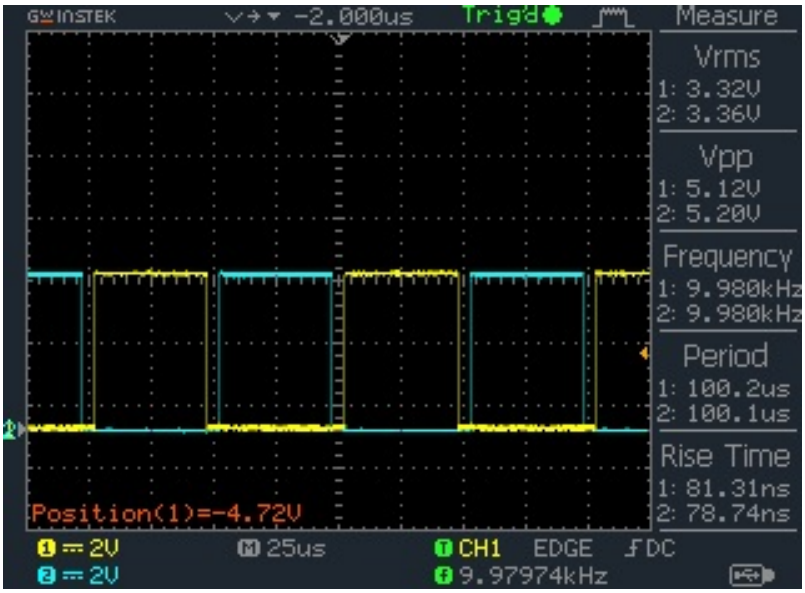

Figure 6.2: Primary side signal overlap analysis at dead time of 5000ns.

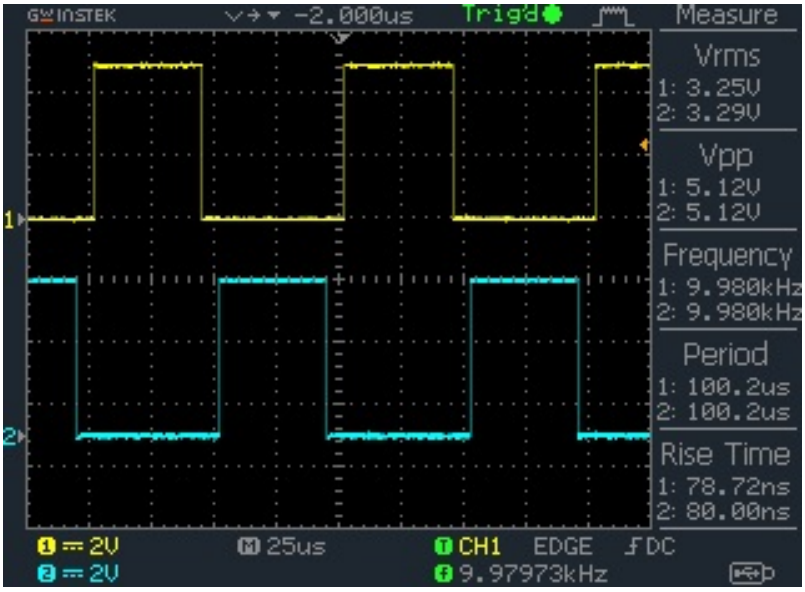

Figure 6.3: Main side changing indicators at 7000 ns dead time..

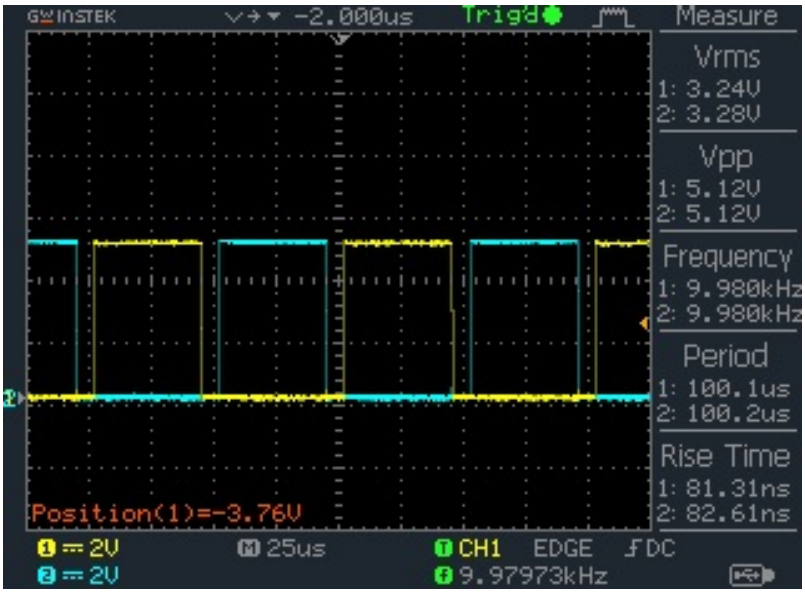

Figure 6.4: This is an overlap analysis of primary side signals at 7000ns dead time..

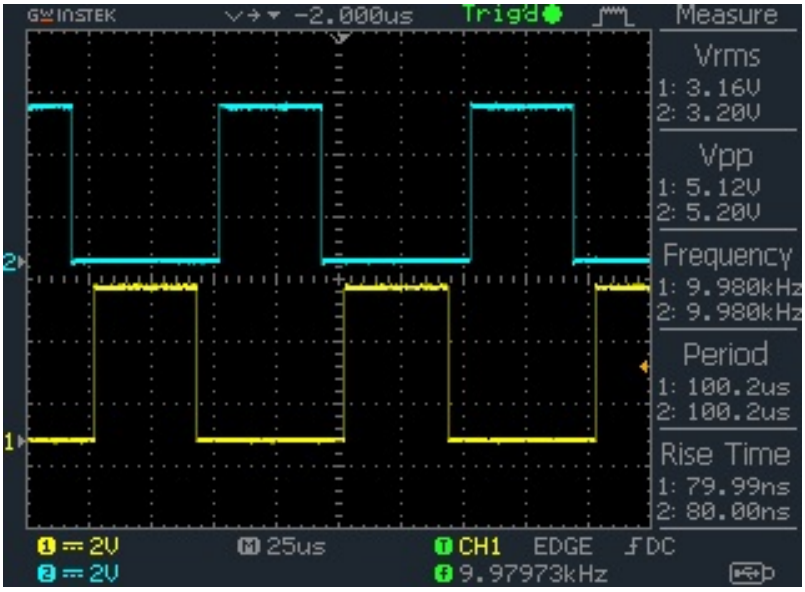

Figure 6.5: Switching signals of the primary side at 9000 ns dead time.

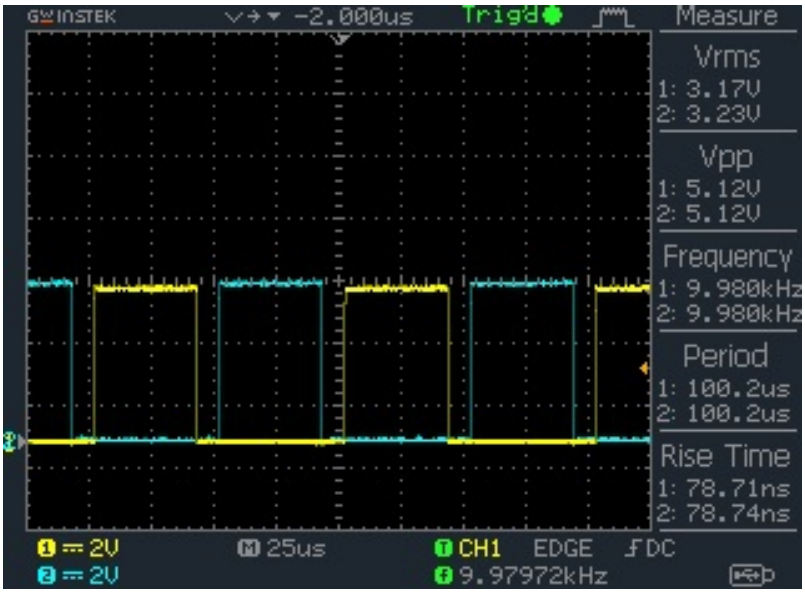

Figure 6.6: Overlap analysis of first side signals at 9000 ns dead time.

6.3 Secondary Side Switching Waveform Analysis

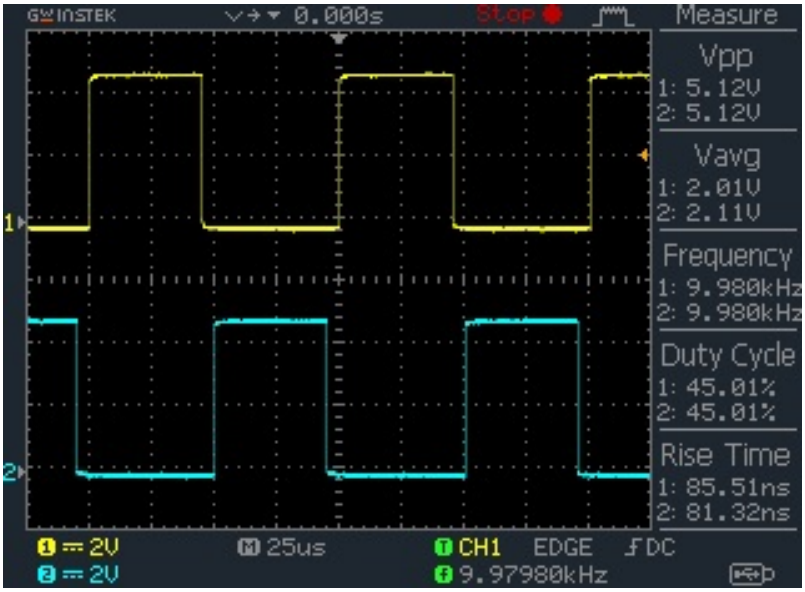

Figure 6.7: Secondary board signals at 5000 ns dead time.

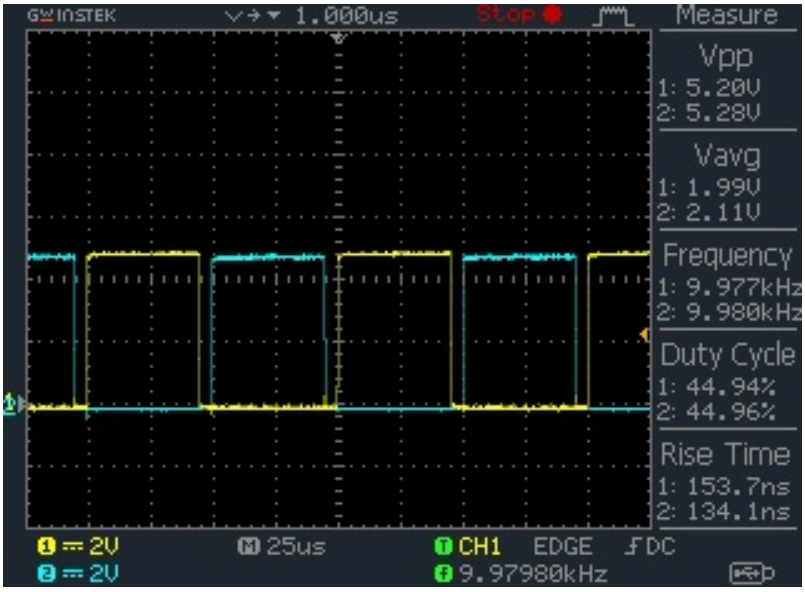

Figure 6.8: Overlap of secondary board signals at 5000 ns dead time.

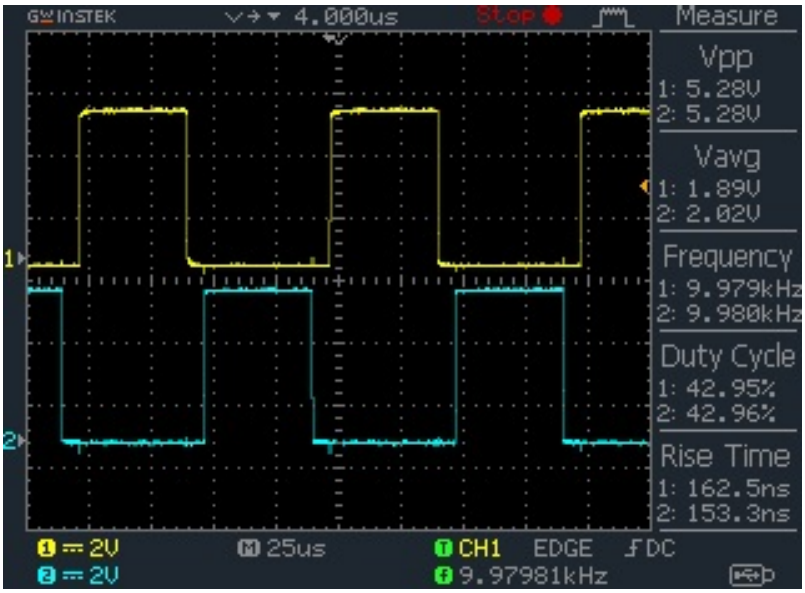

Figure 6.9: Secondary board signals at 7000 ns dead time.

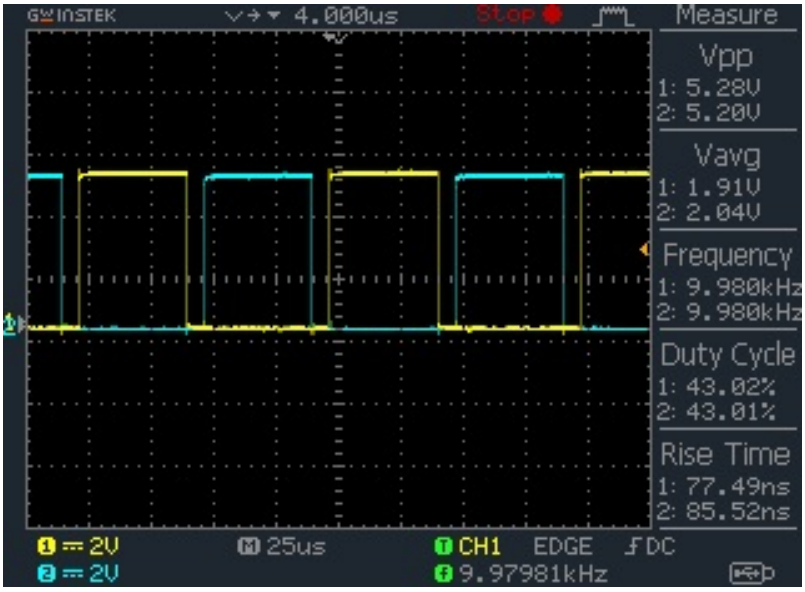

Figure 6.10: Overlap secondary board signals at 7000 ns dead time.

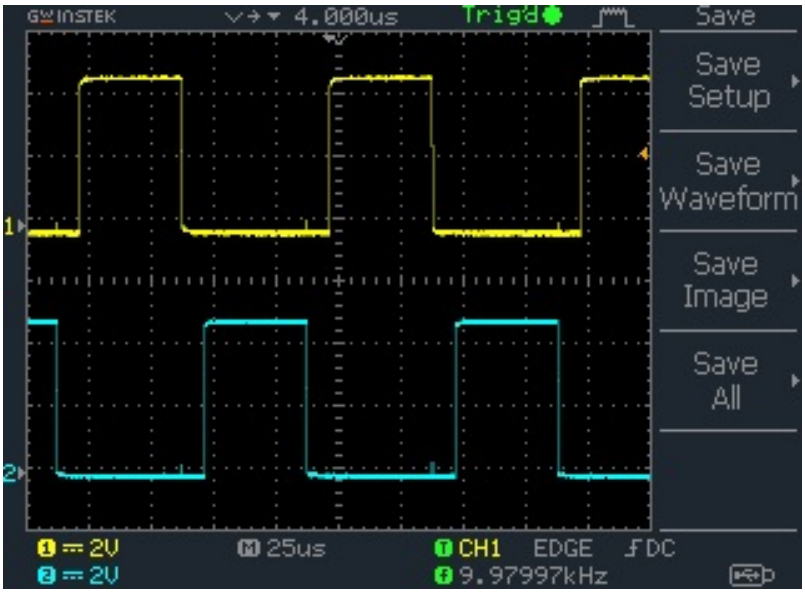

Figure 6.11: Secondary signals at 9000 ns dead time.

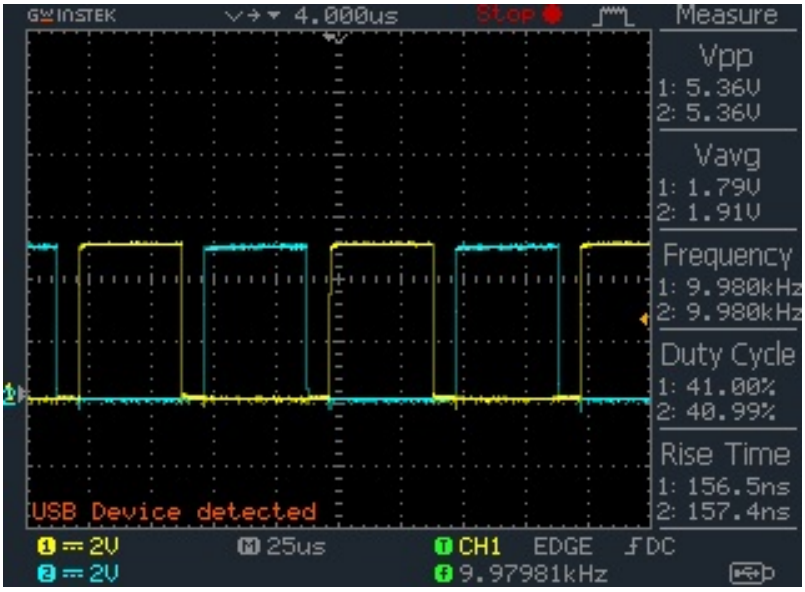

Figure 6.12: Overlap secondary side at 9000 ns dead time.

6.4 Summary

Table **??** summarises the measured performance metrics at different dead-time values, benchmarked against the efficiency targets reported by Krismer and Kolar [4] (89.6% average for SPS modulation on the 1000W prototype) and He and Khaligh .

6.5 Evaluation Discussion

The results demonstrate that ZVS is achievable within the tested dead-time range for the designed converter. As predicted by Shi et al. [8] and confirmed analytically by Everts [9], increasing dead time beyond the optimal value results in incomplete resonant charging of MOSFET output capacitances. The prototype exhibits good agreement with simulation waveforms, validating the MATLAB/Simulink simulation methodology against the analytical framework in [2].

The measured efficiency is compared against the benchmark of Krismer and Kolar [4], who report 89.6% average efficiency for SPS modulation on

the 2 kW automotive DAB prototype (with the same turns ratio $n = 19$ and $L_s = 26.7\,\mu\text{H}$). Deviations from this benchmark are attributed to: (i) non-ideal transformer leakage inductance, (ii) gate drive propagation delay, and (iii) resistive losses in the load bank. These are consistent with loss mechanisms documented in [16].

Limitations of this project include:

- Fixed SPS modulation; advanced strategies such as TPS or DPS [3] could improve efficiency at light loads. Krismer and Kolar [4] demonstrated that switching from SPS to an optimised modulation scheme raises average efficiency from 89.6% to 93.5%.
- Advanced loss models (core loss, skin effect) from are not incorporated in the simulation.
- The resistive load bank does not replicate the dynamic impedance of a real EV battery .

Chapter 7

Conclusion

This project has been able to prove the design, simulation and hardware realization of a Dual Active Bridge (DAB) DCDC converter to be used in EV charging. Adhering to the design approach of Krismer and Kolar. [2] — specifically the 2 kW automotive prototype with $V_1 = 310$ V, $V_2 = 80$ V, $n = 19$, $L_s = 26.7\,\mu$H, and $f_{sw} = 10$ kHz under SPS modulation [4] — and the implementation guidelines of Hannannavar and Shivalli, the following conclusions can be made:

- The DAB converter is a very appropriate topology in bidirectional, galvanically isolated EV charging, which is substantiated by the vast literature. [7, 12, 13].
- Single Phase Shift (SPS) modulation was effectively designed and tested in simulation and hardware. [3].
- ZVS had been attained over the tested dead-time range (5000 9000 ns) and is in line with the limits of analysis of Shi et al. [8] and the closed-form solution of Everts [9].
- The results of hardware switching waveforms were found to be in good agreement with simulation results and confirmed the design and simulation methodology.
- The custom high-frequency transformer has worked as intended which proves the usability of a toroidal core design in DAB applications.

Future Work

Phase Shift (TPS) or Extended Phase Shift (EPS) modulation to increase the range of the ZVS and enhance efficiency at low loads. Krismer and Kolar have proven that optimised modulation increases average efficiency by about 4 percentage points on the same hardware. [4]. of conduction loss modulation Closed-form minimum-conduction-loss modulation, using the method of Krismer and Kolar. [15].

- Design of a closed-loop voltage/current controller of CC -CV battery charge profiles based on the small-signal model framework of.
- V2G experiment with an actual EV battery pack. [6].
- Eoptimisation of efficiency over a broad voltage conversion range that follows. The recently developed Adaptive Battery Charger is a device that is built on the Dual Active Bridge (DAB) converter, providing an efficient, flexible and high performance solution to the current energy storage and electric vehicle charging needs. The topology of the DAB is much superior in terms of power density, efficiency and safety than conventional charging systems due to the high-frequency isolation and the two-way power flow.

  Adaptive control enables the system to dynamically adapt charging parameters to the conditions of the battery to achieve the best performance of charging, extended battery life, and enhanced reliability. Also, the inclusion of smart algorithms, including machine learning to detect battery type, also improves the system to be autonomous in different battery chemistries.

  The proposed system provides stable voltage regulation, efficient power transfer and lower switching losses at various load conditions as shown by simulation and design analysis. It has a modular and scalable design that has enabled it to be used in a broad spectrum of applications, including low-power portable devices and high-power electric vehicle charging stations.

  Finally, this project highlights the success of integrating cutting-edge power electronics with adaptive control solutions in order to meet the growing need of smart and efficient energy systems, making it a promising solution to future sustainable technologies.

References

[1] Shanghai Metals Market (SMM), "From jan to may in 2025, global electric vehicle deliveries recorded approx. 7.520 mil units, a 32.4% YoY growth," https://news.metal.com/newscontent/103409402, July 2025, source: SNE Research. Accessed: 2026-04-28.

[2] F. Krismer, "Modeling and optimization of bidirectional dual active bridge DC–DC converter topologies," Ph.D. dissertation, ETH Zürich, 2010, DISS. ETH NO. 19177.

[3] H. Bai and C. Mi, "Eliminate reactive power and increase system efficiency of isolated bidirectional dual-active-bridge DC–DC converters using novel dual-phase-shift control," *IEEE Transactions on Power Electronics*, vol. 23, no. 6, pp. 2905–2914, 2008.

[4] F. Krismer and J. W. Kolar, "Efficiency-optimized high-current dual active bridge converter for automotive applications," *IEEE Transactions on Industrial Electronics*, vol. 59, no. 7, pp. 2745–2760, 2012.

[5] M. Yilmaz and P. T. Krein, "Review of battery charger topologies, charging power levels, and infrastructure for plug-in electric and hybrid vehicles," *IEEE Transactions on Power Electronics*, vol. 28, no. 5, pp. 2151–2169, 2013.

[6] S. Inoue and H. Akagi, "A bidirectional isolated DC–DC converter as a core circuit of the next-generation medium-voltage power conversion system," *IEEE Transactions on Power Electronics*, vol. 22, no. 2, pp. 535–542, 2007.

[7] R. W. A. A. D. Doncker, D. M. Divan, and M. H. Kheraluwala, "A three-phase soft-switched high-power-density DC/DC converter for high-power applications," *IEEE Transactions on Industry Applications*, vol. 27, no. 1, pp. 63–73, 1991.

[8] H. Shi, H. Wen, J. Chen, Y. Hu, L. Jiang, G. Chen, and J. Ma, "Minimum-reactive-power scheme of dual-active-bridge DC–DC converter with three-level modulated phase-shift control," *IEEE Transactions on Power Electronics*, vol. 35, no. 6, pp. 6409–6424, 2020.

[9] J. Everts, "Closed-form solution for efficient ZVS modulation of DAB converters," *IEEE Transactions on Power Electronics*, vol. 32, no. 10, pp. 7561–7576, 2017.

[10] N. Hou, W. Song, and M. Wu, "Minimum-current-stress scheme of dual active bridge DC–DC converter with unified phase-shift control," *IEEE Transactions on Power Electronics*, vol. 31, no. 12, pp. 8552–8561, 2016.

[11] X. Wu, G. Mu, X. He, and X. Deng, "Unified optimal control strategy based on reference current optimization for bidirectional dual active bridge DC–DC converter," *IEEE Transactions on Power Electronics*, vol. 36, no. 10, pp. 11 468–11 480, 2021.

[12] M. N. Kheraluwala, R. W. Gascoigne, D. M. Divan, and E. D. Baumann, "Performance characterization of a high-power dual active

bridge DC-to-DC converter," *IEEE Transactions on Industry Applications*, vol. 28, no. 6, pp. 1294–1301, 1992.

[13] B. Zhao, Q. Song, W. Liu, and Y. Sun, "Overview of dual-active-bridge isolated bidirectional DC–DC converter for high-frequency-link power-conversion system," *IEEE Transactions on Power Electronics*, vol. 29, no. 8, pp. 4091–4106, 2014.

[14] J. Huang, Y. Wang, Z. Li, and W. Lei, "Unified triple phase shift control of isolated bidirectional DC–DC converter to minimize current stress," *IEEE Transactions on Industrial Electronics*, vol. 69, no. 5, pp. 4648–4659, 2022.

[15] F. Krismer and J. W. Kolar, "Closed form solution for minimum conduction loss modulation of DAB converters," *IEEE Transactions on Power Electronics*, vol. 27, no. 1, pp. 174–188, 2012.

[16] A. Shakoor, A. U. Haq, and T. Iqbal, "Development and evaluation of a high-frequency toroidal transformer for solid-state transformer applications," vol. 45, no. 1, p. 11, 2023.

[17] B. Zhao, Q. Song, W. Liu, and Y. Sun, "Overview of dual-active-bridge isolated bidirectional DC–DC converter for high-frequency-link power-conversion system," *IEEE Transactions on Power Electronics*, vol. 39, no. 4, pp. 4181–4196, 2024.

Appendix A

User Manual

This appendix is a user manual on how to set up and operate the DAB converter prototype, in compliance with safety and operational guidelines in line with. [2].

A.1 Hardware Setup

1. Verify all connections between the primary H-bridge, transformer, secondary H-bridge, and load.
2. Connect the DC power supply to the primary side terminals. Set voltage to 340 V (nominal HV port voltage per [4]).
3. Connect the resistive load bank to the secondary side terminals (12 V nominal).
4. Connect oscilloscope probes to the gate drive test points and inductor current sense resistor.

A.2 Microcontroller Programming

1. Connect the microcontroller via USB to the programming PC.
2. Open the project in STM32CubeIDE.
3. Set the desired dead time in the configuration file (e.g., `DEAD_TIME_NS = 5000`).
4. Compile and flash the firmware.

A.3 Operating Procedure

1. Power on the microcontroller before enabling the DC supply.
2. Enable the DC supply and ramp to rated voltage slowly.
3. Observe gate signals on the oscilloscope to verify correct dead time [8].

4. Record output voltage and current.

5. For V2G mode, negate ϕ in firmware to reverse power flow [3, 7].

A.4 Safety Precautions

- Always wear insulated gloves when handling live circuits.
- Set DC supply current limit before powering on.
- Do not exceed rated voltage and current limits from Table 3.1.
- Discharge bulk capacitors before disassembling the circuit.